European Polymer Journal 250 (2026) 114688

Contents lists available at ScienceDirect

European Polymer Journal

journal homepage: www.elsevier.com/locate/europolj

Research Insights

Structure-property relationships in multi-crystalline PCL/PBS networks: Influence of architecture on one-way and two-way shape-memory behavior

Daniele Natali [a], Chiara Gualandi [b,c,d], Michele Bianchi [e], Andrea Alessandrini [f,g], Stefano Pandini [h], Michele Zanoni [b], Maria Letizia Focarete [b,c,i], Maurizio Toselli [a,c,*]

[a] Department of Industrial Chemistry "Toso Montanari", University of Bologna, Via Piero Gobetti 84, 40129 Bologna, Italy
[b] Department of Chemistry "Giacomo Ciamician", University of Bologna, Via Piero Gobetti 84, 40129 Bologna, Italy
[c] INSTM, UdR of Bologna 40129, Italy
[d] Interdepartmental Center for Industrial Research on Advanced Applications in Mechanical Engineering and Materials Technology (CIRI-MAM), University of Bologna 40136 Bologna, Italy
[e] Department of Life Sciences, University of Modena e Reggio Emilia, Via Giuseppe Campi, 287, 41125 Modena, Italy
[f] Department of Physics, Informatics and Mathematics, University of Modena and Reggio Emilia, Via Giuseppe Campi 213, 41125 Modena, Italy
[g] CNR-Nanoscience Institute-S3, University of Modena and Reggio Emilia, 41125 Modena, Italy
[h] Department of Mechanical and Industrial Engineering, University of Brescia, Via Branze 38, 25133 Brescia, Italy
[i] Health Sciences and Technologies – Interdepartmental Center for Industrial Research (HST-ICIR), University of Bologna 40136 Bologna, Italy

ARTICLE INFO

Keywords:
Shape-memory polymers
Multi-crystalline networks
Poly(ε-caprolactone)
Poly(butylene succinate)
Photo-crosslinked semicrystalline polymers

ABSTRACT

Chemically crosslinked semicrystalline networks containing multiple crystalline phases can display advanced shape-memory behavior, including multi-step one-way transitions and stress-free two-way actuation. Here, network architecture is systematically correlated with these properties in photo-crosslinked systems based on poly(ε-caprolactone) (PCL) and poly(butylene succinate) (PBS). Two series of photo-crosslinked networks were prepared: blends of dimethacrylated PCL and PBS macromonomers, and dimethacrylated PCL-PBS-PCL triblock copolymers. DSC and polarized optical microscopy show that blend networks feature well-segregated PCL and PBS phases that crystallize independently, whereas copolymer networks undergo largely coincident crystallization of the two blocks, leading to broader melting signals and modified crystallization pathways. These distinct thermal and morphological features strongly affect performance: blend networks exhibit excellent triple-shape-memory behavior with clearly separated recovery steps linked to the melting of the two phases. In contrast, copolymer networks uniquely display efficient two-way stress-free actuation, enabled by covalent interphase connectivity that enhances stress transfer during crystallization-induced elongation. This study clarifies how network constitution dictates the balance between multi-step one-way SME and reversible actuation in multi-crystalline polymer networks.

1. Introduction

Shape memory polymers (SMPs) have been extensively studied due to their ability to switch from one or more temporary shapes, in which they have been programmed, to an original or permanent shape, either reversibly or irreversibly, upon exposure to an appropriate stimulus. [1–4] The most recognized effect among these is the one-way shape memory effect (1W-SME), which involves an irreversible, unidirectional change from a temporary shape to a permanent one. To introduce reversibility into this effect, thereby enabling repeated and bidirectional transitions between two predetermined shapes, researchers have explored the two-way shape memory effect (2W-SME).[5,6] This effect can be achieved through the careful application of cooling and heating cycles, combined with the application of an external load in semi-crystalline polymer networks. Currently, most 2W-SMPs are composed of semicrystalline polymer networks. Initial studies have demonstrated that mechanical stress primarily directs the crystallization of polymer chains along the direction of the applied force, thereby leading to observable phenomena such as cold expansion due to crystallization-induced elongation (CIE), and thermal contraction due to melting-induced contraction (MIC). The CIE and MIC mechanisms in semi-crystalline networks are essential prerequisites for the manifestation of

* Corresponding author at: Department of Industrial Chemistry "Toso Montanari", University of Bologna, Via Piero Gobetti 84, 40129 Bologna, Italy.
E-mail address: maurizio.toselli@unibo.it (M. Toselli).

https://doi.org/10.1016/j.eurpolymj.2026.114688
Received 8 January 2026; Received in revised form 3 March 2026; Accepted 25 March 2026
Available online 27 March 2026

2W-SME. Importantly, even in the absence of externally imposed stress, it is necessary to introduce some form of internal stress within the polymeric network, leading to anisotropic crystallization behavior despite the lack of external mechanical forces. Different strategies have been developed for designing shape-memory polymers; among these, the preparation of chemically crosslinked semicrystalline polymeric systems is widely adopted, due to their versatility and the diverse shape-memory properties they can exhibit.[7]

In particular, polymeric networks containing more than one crystalline phase are attracting increasing interest in the field of shape-memory polymers, owing to their unique structure that enables reversible stress-free and multiple shape-memory effects (SMEs). In these systems, a stress-free two-way SME can occur when one crystalline phase acts as a structural skeleton providing internal stress, while the other crystalline phase serves as the actuation domain, allowing the material to change shape through reversible cycles of CIE and MIC. Lendlein et al. [8] were the first to demonstrate a stress-free two-way mechanism in a multiphase copolyester urethane network composed of poly(ω-pentadecalactone) (PDL) and poly(ε-caprolactone) (PCL), which feature two distinct crystallizable chain segments. In this system, the PDL phase forms the skeleton and induces reversible CIE in the PCL phase. Subsequently, Wang et al.[9] synthesized crosslinked copolymers consisting of cocrystallizable monomeric units of PCL and PDL, which exhibited two-way shape memory behavior under both stress and stress-free conditions. Their studies focused on the morphological evolution of these materials during two-way shape-memory cycles, correlating microstructural changes with macroscopic performance. Later, Lai and co-workers investigated the reversible motion in stress-free conditions of crosslinked blends of olefin block copolymers and PCL at different blend compositions [10] and blends composed of PCL and thermoplastic polyurethane (TPU).[11] More recently, Inverardi et al. [12] developed crosslinked polymer networks based on blends of PCL and polyethylene glycol, thoroughly investigating how network composition influences the two-way mechanism in both stress-free and stress-applied scenarios. In a subsequent study, Guo and co-workers [13] introduced an innovative solvent-content-controlled strategy for the preparation of cocrystallizable, photo-curable polyester networks based on PCL and poly(ω-pentadecalactone), enabling an enhanced, stress-free shape-memory response.

In multi-crystalline networks, one-way multiple shape-memory effects are also possible. In these systems, each crystalline domain can serve as a temporary physical netpoint, allowing the material to be fixed in several temporary shapes and to revert to its original shape through multi-step recovery, switching from one temporary shape to another. For example, Cuevas et al. [14] described a triple-shape memory effect in crosslinked blends based on poly(cyclooctene) and polyethylene. Molavi et al.[15] reported similar behavior for biodegradable polylactic acid (PLA)/PCL blends, while Wang et al.[16] also introduced self-healing and photo-responsive capabilities in shape-memory PLA-PCL systems. Although these distinct shape-memory behaviors are well documented, the efficiency and reversibility of the shape-memory response may be significantly affected by the constitution of the polymer network and the microstructure of the crystalline domains. However, despite the growing interest in multi-crystalline systems, a direct comparison between stress-free two-way actuation and one-way multiple shape-memory behavior within networks built from the same polymer segments is still lacking. Closing this gap is essential for elucidating how network constitution and composition govern shape-memory performance and for establishing structure–property relationships that support the rational design of multifunctional shape-memory materials.

In this work, multi-crystalline crosslinked networks composed of the same polymeric segments arranged into different topologies were synthesized to investigate how the network's chemical structure affects shape-memory properties, specifically stress-free two-way and one-way multiple-SMEs. Poly(ε-caprolactone) (PCL) and polybutylene succinate (PBS) were selected as the semicrystalline components. The former has been widely employed in shape memory polymers [9–13] as the actuation phase of multi-crystalline networks due to its low melting temperature and fast crystallization rate,[17] whereas PBS exhibits higher melting and crystallization temperatures compared to PCL.

Chemically crosslinked networks were produced using two complementary approaches: (i) blending photo-crosslinkable PCL and PBS homopolymers in various ratios to generate networks with different compositions; and (ii) employing photo-crosslinkable PCL-PBS-PCL triblock copolymers of varying block lengths. The first approach yields networks in which PBS and PCL chains are crosslinked at their terminal ends, with the resulting morphology influenced by the miscibility between the two homopolymers. In contrast, the second approach produces architectures in which blocks of PCL and PBS are covalently linked, with crosslinking points formed by the terminal reactive groups of the PCL end blocks in the triblock copolymers. The thermal and shape-memory properties of these networks were systematically investigated to elucidate how changes in polymer constitution, morphology, and crystalline phase organization affect both reversible stress-free and one-way multiple shape-memory responses in semicrystalline networks.

2. Experimental section

2.1. Materials

Poly(ε-caprolactone) diol (number average molecular weight $M_n \approx$ 10 kDa, PCL10), dimethyl succinate, 1,4-butanediol, 2-isocyanatoethyl methacrylate (2-IEM, 98%), titanium(IV) butoxide (97%), tin(II) 2-ethylhexanoate ($Sn(Oct)_2$), calcium hydride (CaH_2), chloroform, and methanol were purchased from Sigma-Aldrich and used as received, without further purification. 2-hydroxy-2-methyl-1-phenyl propanone (HMPP) was purchased from Cytec and used as photoinitiator. ε-caprolactone (CL, 97%) was purchased from Merck and purified prior to use by distillation under reduced pressure in the presence of molecular sieves and CaH_2.

2.2. Synthesis of poly(butylene succinate) diols

Hydroxyl-terminated PBS diols were synthesized by a two-step bulk polycondensation of dimethyl succinate and 1,4-butanediol, following literature procedures (Scheme 1a).[18] In the first step, the monomers were reacted at 160 °C in the presence of titanium(IV) butoxide to promote transesterification, using a 15% molar excess of 1,4-butanediol with respect to dimethyl succinate. The reaction mixture was then heated to 240 °C and subjected to reduced pressure to drive the polycondensation step, yielding PBS diols with number-average molecular weights of approximately 4 kDa (PBS4) or 10.5 kDa (PBS10.5), as determined by ^{1}H NMR analysis (Equation 2). No further purification was performed on the crude products. For a typical synthesis, 58.5 g (0.40 mol) of dimethyl succinate were added to a 250 mL three-neck round-bottom flask with 41.5 g of 1,4-butanediol (0.46 mol). The mixture was stirred magnetically under a nitrogen atmosphere by raising the temperature to 160 °C. Titanium(IV) butoxide (0.068 g, 0.20 mmol) was added to the reaction mixture. After 2 h, the temperature was raised to 240 °C, an additional 0.068 g (0.20 mmol) of titanium(IV) butoxide was added, and vacuum was applied.

2.3. Synthesis of PCL-PBS-PCL triblock copolymers

Hydroxyl-terminated PCL–PBS–PCL copolymers were prepared via ring-opening polymerization of ε-caprolactone initiated by PBS4 diols in the presence of tin(II) 2-ethylhexanoate at 130 °C under nitrogen (Scheme 1b). By varying the CL/PBS4 feed ratio, a series of triblock copolymers was obtained with PCL block M_n between 2.7 and 9.0 kDa and PCL contents from 57 to 82 wt%, as calculated from ^{1}H NMR spectra using Equation 3 (see Table 1 for the values corresponding to samples C_1 − C_4). In brief, after drying PBS4 at 60 °C under vacuum overnight,

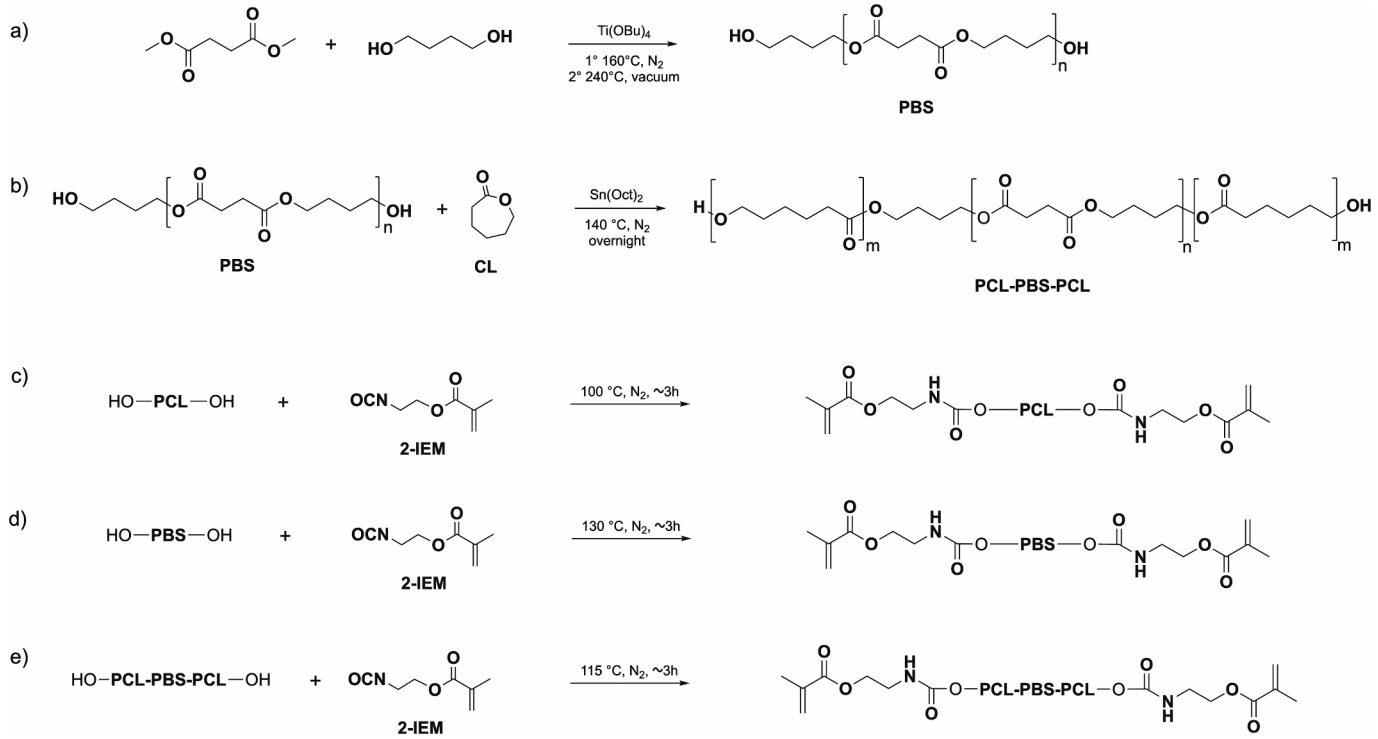

Scheme 1. Reaction schemes: a) synthesis of PBS from dimethyl succinate and 1,4-butanediol; b) synthesis of PCL-PBS-PCL triblock copolymer; c) methacrylation of the hydroxyl terminal groups of PCL; d) methacrylation of the hydroxyl terminal groups of PBS; e) methacrylation of the hydroxyl terminal groups of PCL-PBS-PCL triblock copolymer.

the synthesis was performed by reacting freshly distilled CL with PBS4 diol at 130 °C for at least 12 h in the presence of $Sn(Oct)_2$ as a catalyst (Scheme 1b). For example, to prepare the triblock copolymer used in the network denoted as C_4 (Table 1), 3.40 g of PBS4 diol (0.86 mmol) were placed in a three-neck round-bottom flask equipped with a mechanical stirrer and melted at 130 °C. Afterward, 16.4 g of CL (144 mmol) and 0.020 g of $Sn(Oct)_2$ (0.1 wt%) were added, and the reaction was carried out overnight under nitrogen atmosphere.

2.4. Methacrylation of polyesters

Methacrylation of the hydroxyl terminal groups of PCL and PBS diols, as well as PCL-PBS-PCL triblock copolymers, was performed in bulk with 2-isocyanatoethyl methacrylate (2-IEM) according to published protocols (Scheme 1c,d,e).[19] PCL diol was dried under vacuum in the presence of molecular sieves at 45 °C before use, whereas PBS10.5 and PCL-PBS-PCL triblock copolymers were functionalized directly using a one-pot reaction immediately after their synthesis. In all cases, 2-IEM was used in a 20% molar excess with respect to hydroxyl groups, and unreacted 2-IEM was removed under dynamic vacuum at the end of the reaction, as confirmed by the disappearance of the isocyanate band at 2275 cm^{-1} in FT-IR spectra.

For PCL diol, methacrylation was carried out in bulk at 100 °C for about 3 h under nitrogen and mechanical stirring, whereas PBS10.5 and PCL–PBS–PCL copolymers were functionalized at 130 °C and 115 °C, respectively. Due to the higher reaction temperature, 250 ppm of BHT inhibitor was added for PBS10.5 to prevent premature crosslinking, and this material was purified by dissolution in chloroform and precipitation in cold methanol, while PCL and PCL–PBS–PCL derivatives were used without further purification. The degree of methacrylation of all macromonomers, determined by ^{1}H NMR (Equation 4), was $\geq$ 97–98%, indicating nearly quantitative end-group functionalization.

2.5. Preparation of chemically crosslinked networks

Two series of photo-crosslinked networks were prepared from the methacrylated macromonomers. The first set, denoted B, was obtained by photopolymerization of molten blends of methacrylated PBS10.5 and PCL10 homopolymers at different weight ratios (Table 1). In this preparation, the blends were melted at 130 °C, then thoroughly mixed with 0.5 wt% HMPP, which served as the radical photoinitiator. The second set, denoted C, was prepared by melting methacrylated PCL–PBS–PCL triblock copolymers at 130 °C with 0.5 wt% HMPP (Table 1). In both cases, the molten formulations were poured between glass plates (25 mm × 75 mm) separated by polytetrafluoroethylene spacers (thickness: 0.3–0.4 mm) to form films. Photo-crosslinking was carried out on a heated plate using a 365 nm UV lamp (Hamamatsu spot light source LC8), positioned at approximately 12 cm from the samples and delivering an intensity of 6 mW cm^{-2}. Both sides of each sample were irradiated for 5 min. Free-standing films with a thickness of about 400 μm were obtained by detaching them from the glass plates and subjecting both sides to an additional 5 min UV post-cure to ensure complete crosslinking.

2.6. Chemical characterization

Fourier transform infrared spectroscopy (FT-IR) was performed using a PerkinElmer FT-IR system, model Spectrum Two, operating in Attenuated Total Reflection (ATR) mode, using 32 scans at a resolution of 4 cm^{-1}. ^{1}H NMR spectra were acquired in $CDCl_3$ at 300 MHz using a Mercury 300 spectrometer, with chemical shifts referenced to tetramethylsilane at 0 ppm.

The number-average molecular weight (M_n) of commercial hydroxyl-terminated PCL (nominal ≈ 10 kDa) was determined from the ^{1}H NMR peak integrals using Equation 1:

$$M_n\,(\mathrm{PCL}) = 104 + \left(\frac{A^{2.30}}{A^{3.65}} \times 114 \times 2\right) \quad [1]$$

where $A^{2.30}$ and $A^{3.65}$ are the integrals of the signals centered at 2.30 and 3.65 ppm, respectively (spectra and assignments in Fig. S1), and 104 and 114 correspond to the molecular weight of the diethylene glycol initiator and of the caprolactone repeating unit, respectively. Similarly, the number-average molecular weight (M_n) of hydroxyl-terminated PBS was calculated from ^{1}H NMR data according to Equation 2, following a reported procedure [18]:

$$M_n(\text{PBS}) = 90 + \frac{A^{4.10}}{A^{3.65}} \times 172 \quad [2]$$

where $A^{4.10}$ and $A^{3.65}$ are the integrals of the signals centered at 4.10 and 3.65 ppm, respectively (spectra and assignments in Fig. S2), 90 is the molecular weight of the terminal butanediol unit, and 172 is the molecular weight of the butylene succinate repeating unit.

The PCL-PBS-PCL triblock copolymers were synthesized via the ring-opening polymerization of ε-caprolactone initiated by the terminal hydroxyl groups of PBS4. At the end of the reaction, ^{1}H NMR analysis confirmed the complete consumption of caprolactone. The number-average molecular weight (M_n) of the PCL block in the triblock copolymers was determined according to the following equation:

$$M_n\,(\text{PCL block}) = \frac{A^{2.30}}{A^{2.62}} \times DP_{PBS} \times 114 \quad [3]$$

where $A^{2.30}$ and $A^{2.62}$ are the integrals of the signals centered at 2.30 ppm and 2.62 ppm, respectively (Fig. S3), DP_{PBS} is the average degree of polymerization of the starting PBS diol (22 for the PBS4), and 114 is the molecular weight of the CL repeating unit. These values describe the average size of each PCL block in the copolymer and are consistent with those calculated from the initial PBS/CL stoichiometric composition, assuming complete conversion of the CL monomer.

The degree of methacrylation (D_M) of PCL, PBS and PCL-PBS-PCL triblock copolymers was investigated by ^{1}H NMR and expressed according to the following equation reported by Messori et al.:[19]

$$D_M(\%) = \frac{A^{3.50}}{A^{3.50} + A^{3.65}} \times 100 \quad [4]$$

where $A^{3.50}$ and $A^{3.65}$ are the area of the signals centered at 3.50 ppm and 3.65, respectively (Figs. S4-S6). The disappearance of this latter signal confirms the complete functionalization of the polymers. All the prepared methacrylated polymers and copolymers exhibited a $D_M \geq$ 97–98%.

2.7. Thermal, thermo-mechanical and morphological characterization

The thermal properties of the samples were analyzed by differential scanning calorimetry (DSC) using a TA Instruments Q2000 DSC, equipped with a refrigerated cooling system. Each specimen underwent a first heating scan at a rate of 20 °C min^{-1} from −40 °C to 160 °C, followed by a controlled cooling at the same rate of 20 °C min^{-1} down to −40 °C, and a second heating scan at 20 °C min^{-1} up to 140 °C, all performed in a nitrogen atmosphere. The crystallinity content of PCL and PBS domains was calculated by applying Equation 5, considering the values of specific melting enthalpy for the 100% crystalline *i*-phase.

$$\chi_c = \frac{\Delta H_{m,i}}{\Delta H^0_{m,i}} \frac{1}{w_i} \times 100 \quad [5]$$

where $\Delta H_{m,i}$ is the melting enthalpy of the *i*-phase (either PBS or PCL) in the second heating scan, $\Delta H^0_{m,i}$ is the specific melting enthalpy for the 100% crystalline *i*-phase (200 J g^{-1} for PBS [20] and 135 J g^{-1} for PCL [21]), and w_i is the weight percentage of the *i*-phase (PBS or PCL) in the sample.

The photo-crosslinked samples were also characterized in terms of gel fraction. Specimens with initial mass m_0 and square shape (about 10 × 10 mm^2) were placed in 10 mL of chloroform overnight at room temperature. After that, the swollen sample was dried at room temperature until a constant weight was reached to measure the residual mass of the sample after extraction (m_d). The gel content (G), reported in Table S1, was determined as the average value obtained from three specimens, according to the following equation:

$$G = \frac{m_d}{m_0} \times 100 \quad [6]$$

Polarized optical microscopy (Zeiss Axio Observer, Linkam hot stage) was employed to investigate the crystallization behavior of photo-crosslinked samples. Methacrylate polymers were melted, pressed firmly between two glass slides, and photo-crosslinked at 130 °C to obtain very thin films. Crystalline phase evolution was assessed by adapting the method reported by Huang and coworkers.[22] Briefly, the films were heated at 130 °C to fully melt PBS and PCL crystalline domains, then slowly cooled at a controlled rate to monitor crystalline phase formation. Upon onset of crystallization, samples were maintained under isothermal conditions to enable complete crystalline growth.

Dynamic mechanical thermal analysis (DMTA) was performed on rectangular film strips (gauge length 10 mm, width ≈ 5 mm) in tensile mode using a DMA Q800 (TA Instruments). Measurements were carried out under a controlled thermal cycle to investigate the viscoelastic response of the material. The specimens were first equilibrated at 150 °C and then cooled from 150 °C to 0 °C at 3 °C min^{-1}, followed by a subsequent heating ramp from 0 °C to 150 °C at the same rate. Throughout the thermal cycle, an oscillatory tensile strain with an amplitude of 0.5% at 1 Hz was applied under displacement-controlled mode.

Sample morphology was also characterized by atomic force microscopy (AFM). AFM imaging was performed using a Bioscope equipped with a Nanoscope IIIA controller (Veeco Metrology, USA) in tapping mode with RTESPA-300 cantilevers (Bruker, CA, USA; tip resonance frequency ≈ 300 kHz). Images were obtained from the free surface of the photo-crosslinked films, acquiring both the topographic and the phase signal, in the as-prepared state and after uniaxial elongation. All images were plane fitted with a third-order subtraction, and phase images underwent a low-pass filtering with a 3 x 3 matrix.

2.8. Shape-memory characterization

Shape memory behavior was assessed using a DMA Q800 (TA Instruments) on rectangular strips (gauge length: 10 mm; width: ≈5 mm) under tensile mode. The one-way triple-shape memory effect was evaluated by subjecting the specimen to the following thermo-mechanical protocol: i) heating (original permanent shape, O) to the programming temperature (T_{pr}), defined as $T_{m,PBS}$ + 30 °C (T_{pr} = 140 °C for B samples and 120 °C for C samples); ii) stretching to 25% of strain; iii) fixing the first temporary shape (Shape I) by cooling down to 65 °C (below $T_{c,PBS}$, above $T_{m,PCL}$); iv) applying a further stretching to 50% total strain; v) cooling under constant strain to −20 °C (below $T_{c,PCL}$) to fix the second temporary shape (Shape II); vi) unloading the sample (down to a minimum load equal to 0.01 N). One-way triple-shape SME was assessed by heating the sample at 2 °C min^{-1} to T_{pr}. The shape fixity parameter, R_{fix}, for the second, and final, temporary shape, was calculated as:

$$R_{fix} = \frac{\varepsilon_{unload}}{\varepsilon_{app}} \times 100 \quad [7]$$

where ε_{unload} is the residual strain of the sample after unloading below $T_{c,PCL}$, and ε_{app} is the total applied strain. The two strain recovery steps, from the second to the first temporary shape ($R_{II\to I}$), and from the first temporary to the original shape ($R_{I\to O}$), were evaluated at $T > T_{m,PCL}$ and $T > T_{m,PBS}$, respectively, by applying Equations 8 and 9:

$$R_{II\to I} = \frac{\varepsilon_{unload} - \varepsilon_1}{\varepsilon_{unload}} \times 100 \quad [8]$$

$$R_{I\to O} = \frac{\varepsilon_1 - \varepsilon_{rec}}{\varepsilon_{unload}} \times 100 \quad [9]$$

where ε_1 is the residual strain after PCL melting, and ε_{rec} is the

residual strain after PBS melting. The overall strain recovery, R_{rec}, was calculated by applying Equation 10:

$$R_{rec} = \frac{\varepsilon_{unload} - \varepsilon_{rec}}{\varepsilon_{unload}} \times 100 \quad [10]$$

For two-way stress-free reversible shape memory effect, the following thermo-mechanical protocol was applied: i) heating the sample to the programming temperature, T_{pr} ($T_{pr} = 140$ °C for B samples; 120 °C for C samples); ii) elongating the sample until a certain pre-strain through the application of a load; iii) cooling to −20 °C (below $T_{c,PCL}$) at 2 °C min^{-1} while maintaining the load; iv) unloading the sample (a minimum load equal to 0.01 N was applied so to avoid buckling of the sample and instability); v) heating the specimen at the so-called activation temperature (T_{act}), defined as $T_{act} = T_{m,PCL} + 15$ °C; vi) cooling from T_{act} to –20 °C, at a scan rate of 2 °C min^{-1}, and vii) heating from –20 °C to T_{act} at a scan rate of 2 °C min^{-1}. The latter cooling and heating cycle (step vi and vii) was repeated up to 5 times, and here the two-way stress-free shape-memory effect was assessed; pristine steps (i-v) may be considered as a training cycle that prepared the specimen for such a response. The elongation strain along the stress-free cycle was defined as the reversible strain, and was quantified with two parameters, ε_{rev} and ε'_{rev}, that were calculated as the average on second to fifth cycle according to Equations 11 and 12:

$$\varepsilon_{rev(2-5)} = \frac{l_{low} - l_{high}}{l_0} \times 100 \quad [11]$$

$$\varepsilon'_{rev(2-5)} = \frac{l_{low} - l_{high}}{l_{high}} \times 100 \quad [12]$$

where l_{low}, is the length of the sample at T_{low} (after the PCL crystallization, at the end of the cooling step vi), l_{high} is the length of the sample at T_{high} (T_{act}, at the end of the heating step vii) and l_0 is the initial length of the sample; more specifically, ε_{rev} represents the average elongation strain that takes place in the stress-free cooling-heating cycle (i.e., referred to the undeformed sample), whereas ε'_{rev} represents the elongational strain normalized to the strain value before the application of the stress-free cooling-heating cycle (i.e., referred to the trained sample).

The stress-driven crystallization-induced elongation (CIE_{SD}) was calculated by Equation 13 and refers to the cooling step of the training phase (step iv), during which the sample is kept under constant load (step iii in the previous thermo-mechanical protocol). In this case, $l_{high,SD}$ is the length of the sample measured just before PCL crystallization (end of step iii), and $l_{low,SD}$ is the length after the steep elongation due to PCL crystallization (end of step iv):

$$CIE_{SD} = \frac{l_{low,SD} - l_{high,SD}}{l_0} \quad [13]$$

3. Results and discussion

3.1. Synthesis of networks

Several methods can be employed to produce chemically crosslinked networks with distinct semicrystalline phases. One approach involves blending crosslinkable semicrystalline macromonomers (AA and BB), followed by an appropriate curing process to obtain a network that integrates both crystalline phases originating from the precursor materials. An alternative strategy employs linear block copolymers (e.g. AA-BB, AA-BB-AA), appropriately functionalized to be crosslinked, containing crystallizable segments.

The photo-crosslinkable macromonomers were synthesized following established protocols described in the literature[19] through the reaction of hydroxyl-terminated polyester diols with an isocyanate containing a methacrylate group (2-IEM). The FT-IR and NMR analysis confirmed the reaction with 2-IEM, as evidenced by the conversion of hydroxyl end-groups and the formation of the expected methacrylated macromonomers. The ^{1}H NMR spectra of PCL, PBS and PCL-PBS-PCL methacrylated macromonomers, in comparison with those of the corresponding pristine polymers and copolymers, are reported with the respective assignments in Figs. S1-S6.

Subsequently, two distinct series of networks were synthesized via photo-crosslinking of these methacrylated macromonomers with varying molecular weights and compositions. The first series, derived from blends of PBS and PCL methacrylated macromonomers, was labeled series “B” (B stands for blends), whereas the second series, obtained from methacrylated PCL-PBS-PCL triblock copolymers, was labeled series “C” (C stands for copolymers). Details regarding composition, macromonomer molecular weight, and the PCL/PBS phase ratio for the obtained networks are summarized in Table 1.

3.2. Thermal properties of crosslinked networks

Thermal analysis of the networks derived from the photo-crosslinking of blends of PBS and PCL macromonomers (B samples) and from PCL-PBS-PCL triblock copolymers (C samples) was performed using DSC. All samples underwent a first heating step up to 160 °C to erase their thermal history, followed by cooling to −40 °C and a second heating to 140 °C at a rate of 20 °C min^{-1}.

Fig. 1 shows the cooling and the second heating scans for both series of networks, in comparison with those obtained from pure PCL10 and PBS10.5 methacrylated macromonomers. The calorimetric data acquired from these thermograms are summarized in Table 2.

The DSC curves of the B_series samples (Fig. 1a,b) display multiple exothermic and endothermic signals in both cooling and heating scans, respectively, indicating the presence of a multi-crystalline structure. In Fig. 1b, which shows the heating scans after controlled cooling, two distinct endothermic peaks are observed in all B samples; the first located around 50 °C and the second is centered at approximately 110 °C. These temperatures closely match the melting points of the neat crosslinked PCL and PBS homopolymers (52 °C and 114 °C, respectively). On this basis, the low-temperature exothermic (cooling scans) and endothermic (heating scans) signals are assigned to PCL crystals, whereas the high-temperature transitions are attributed to PBS crystals.

Notably, the melting enthalpies of both PCL and PBS in B_series networks scale linearly with the relative content of the two polyesters in the networks (Fig. S7), whereas the melting temperatures remain comparable to those of the corresponding homopolymers. This behavior can be rationalized by assuming that blending photo-curable PCL and PBS macromonomers produces a polymer network in which the pronounced immiscibility between the two components dominates over the chemical bonding occurring at the chain ends. As a result, distinct PCL-rich and PBS-rich phases are formed, each crystallizing independently and primarily governed by its own volume fraction. A similar behavior has been

Table 1
Sample code, type of macromonomers and composition of photo-crosslinked networks.

Sample Code	Dimethacrylated macromonomers	$M_{n,PCL}$ [a] (kDa)	$M_{n,PBS}$ [b] (kDa)	PCL/PBS (w/w)
B_1	PCL10 and PBS10.5 homopolymers	9.8	10.5	40/60
B_2				60/40
B_3				75/25
B_4				85/15
C_1	PCL-PBS-PCL triblock copolymers	2.7	4.0	57/43
C_2		3.9		66/34
C_3		6.7		77/23
C_4		9.0		82/18

[a] Determined by ^{1}H NMR analysis using Equation 1 (B_series) and 3 (C_series, the value corresponds to each PCL block).
[b] Determined by ^{1}H NMR analysis using Equation 2.

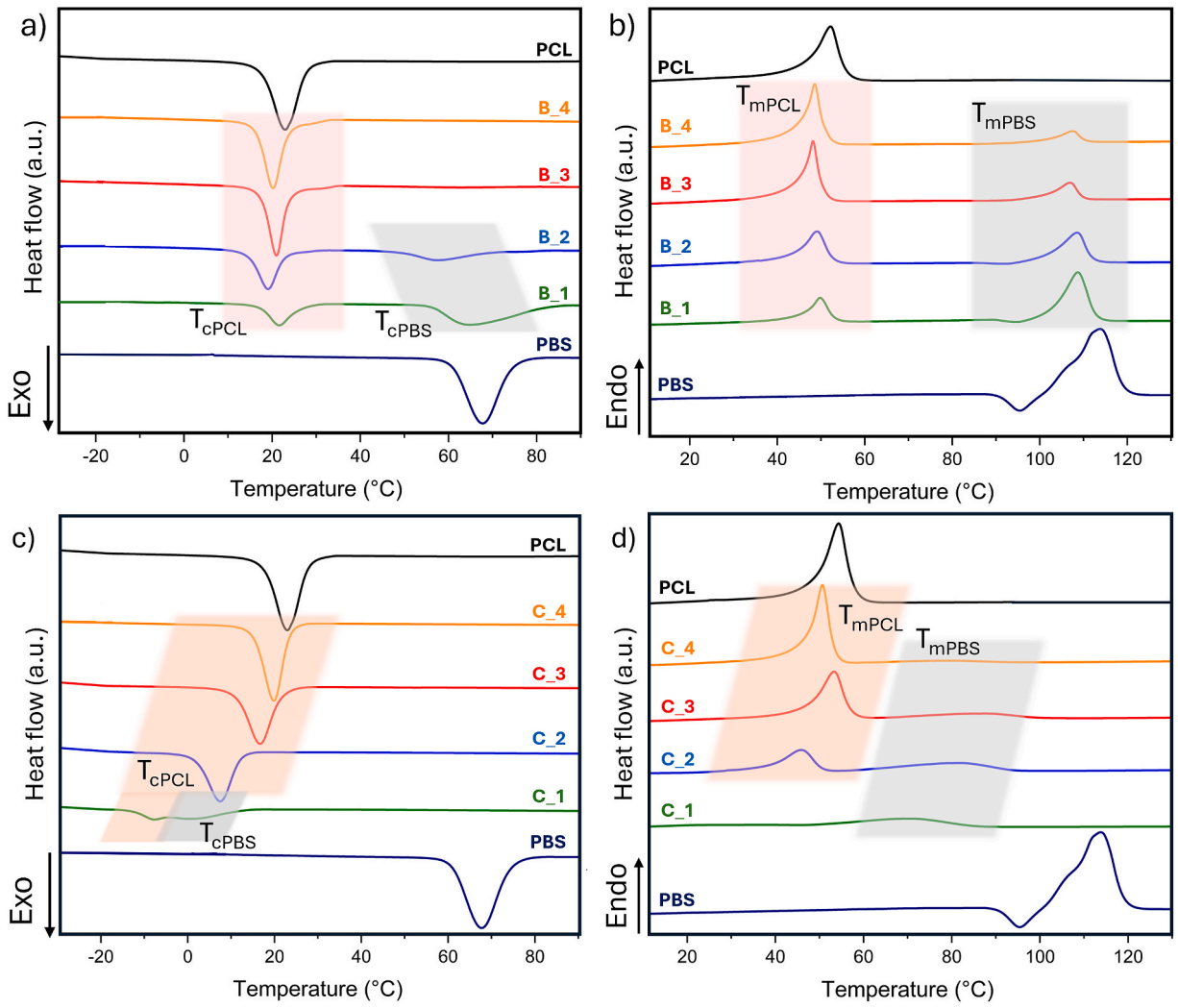

Fig. 1. DSC cooling scans (a, c) and heating scans (b, d) of B (a, b) and C samples (c, d). The curves of the neat crosslinked homopolymers (PCL10 and PBS10.5) are included for comparison. Peaks associated with PCL are highlighted in red, whereas those associated with PBS are highlighted in grey.

Table 2
Thermal analysis of semicrystalline PCL/PBS networks.

Sample code	*Cooling scan*				*2nd heating scan*					
	$T_{c,PCL}$ (°C)	$T_{c,PBS}$ (°C)	$\Delta H_{c,PCL}$ (J g^{-1})	$\Delta H_{c,PBS}$ (J g^{-1})	$T_{m,PCL}$ (°C)	$T_{m,PBS}$ (°C)	$\Delta H_{m,PCL}$ (J g^{-1})	$\Delta H_{m,PBS}$ (J g^{-1})	$X_{c,PCL}$[a] (%)	$X_{c,PBS}$[a] (%)
PCL	21	–	49	–	52	–	46	–	36	–
PBS	–	68	–	66	–	114	–	91	–	46
B_1	22	65	17	38	50	109	18	37	33(13)	31(19)
B_2	19	57	29	17	49	109	29	25	36(22)	31(12)
B_3	18	n.d.	44[b]	n.d.	50	109	40	16	40(30)	32(8.0)
B_4	21	n.d.	52[b]	n.d.	49	108	48	10	42(36)	33(5.0)
C_1	−8	2	−27[c]		n.d	71	n.d	32	n.d.	37(16)
C_2	7	n.d.	37	n.d.	45	82	18	16	21(14)	22(7.5)
C_3	17	n.d.	44	n.d.	53	88	34	9	33(25)	19(4.4)
C_4	20	n.d.	46	n.d.	51	79	44	3	40(33)	9(1.6)

[a] Values determined using Equation 5; the values in parentheses refer to crystallinity calculated with respect to the total mass of the samples (i.e., the values from Equation 5 multiplied by the respective weight fractions given in Table 1).

[b] These values are likely slightly overestimated due to a possible overlap with the PBS crystallization peak (a small shoulder is visible on the right side of the PCL crystallization peak in Fig. 1a for samples B_3 and B_4).

[c] A single value is reported owing to the significant overlap of the peaks (Fig. 1c).

reported for photo-cured semicrystalline dimethacrylated PEG/PCL networks, which show separate melting and crystallization transitions due to the partial immiscibility of the two components.[12]

The crystallinity content of PCL and PBS was determined from the second heating scan using Equation 5 (Table 2). Specifically, the measured melting enthalpies were normalized to the enthalpy of a 100% crystalline phase and corrected for the weight fraction of each phase. In Table 2, the crystallinity values are reported both as phase-normalized

percentages (according to Equation 5) and, in parentheses, as crystallinity calculated with respect to the total sample mass, obtained by multiplying the phase-normalized values by the corresponding weight fractions listed in Table 1, so as to provide the overall crystalline fraction of each phase in the networks.

In B samples, the phase-normalized degree of crystallinity of PCL ($\chi_{c,PCL}$) increases slightly from 33% in the network with the lowest PCL content (B_1) to approximately 40% in the networks with higher PCL content (B_3 and B_4). For comparison, the photo-crosslinked neat PCL exhibits a crystallinity degree of 36%. Conversely, the phase-normalized crystallinity degree of the PBS phase in the B samples decreased from 46%, in the pure crosslinked PBS network to about 32% in the blends, with no apparent dependence on blend composition. This outcome is consistent with the findings reported by Qiu et al.[23] regarding the crystallization behavior of PBS and PCL in blends at different weight ratios. Overall, these results indicate that PCL tends to crystallize more readily than PBS within blend networks. When considering the overall crystalline fractions (values in parentheses in Table 2), B-networks exhibit a total PCL crystallinity increasing from about 13% in B_1 to 36% in B_4, while the PBS crystalline fraction remains in the 5–19% range, reflecting the progressive dominance of PCL crystals at high PCL contents.

The distinct crystallization behavior of the PCL and PBS phases in the B samples is further evidenced by the cooling scans (Fig. 1a). The crystallization temperature of the PCL phase ($T_{c,PCL}$) in these networks remains close to that of the crosslinked neat homopolymer, whereas the crystallization temperature for PBS ($T_{c,PBS}$) decreases markedly as the PCL content in the network increases. In blends with the highest PCL contents (B_3 and B_4), no distinct PBS crystallization peak is detected; however, coincident crystallization of PBS and PCL upon cooling in the same temperature range cannot be excluded. In agreement with the results of Fenni and co-workers,[24] PCL-rich blends may exhibit coincident crystallization of the two semicrystalline components and, consistently with the observations reported by the authors, B_3 and B_4 networks showed a single crystallization peak around $T_{c,PCL}$, while the subsequent heating scan shows two distinct melting peaks, each associated with one of the blend components.

Furthermore, the $\Delta H_{c,PCL}$ values measured for B_3 and B_4 (44 and 52 J g^{-1}, respectively) appear to be overestimated, as they exceed the corresponding $\Delta H_{m,PCL}$ values obtained in the subsequent heating step (40 and 48 J g^{-1}, respectively); this finding supports the hypothesis of coincident crystallization of the two components while cooling at 20 °C min^{-1} in DSC. Notably, even for the blend with the highest PCL content (85 wt% in B_4), in which no PBS crystallization peak is detected upon cooling, a distinct PBS melting peak is observed during the subsequent heating at a temperature very close to that of the PBS homopolymer (Fig. 1b, yellow curve), with a crystallinity degree that is not significantly different from that of the other B samples.

The crystallization and melting behaviors of C samples, prepared through the photo-crosslinking of dimethacrylated PCL-PBS-PCL copolymers with varying PCL block lengths, are showed in Fig. 1c and 1d and summarized in Table 2. In particular, the PCL block length in this series increases from 2.7 kDa in C_1 to 9.0 kDa in C_4 (Table 1), providing a convenient handle to tune the crystallization behavior and, as discussed below, the actuation performance. In Fig. 1c, a single exothermic peak is detected for samples with PCL blocks exceeding 3 kDa (C_2, C_3, and C_4). These peaks, which occur at temperatures below the T_c of the neat PCL network, are attributable to the crystallization of PCL chains ($T_{c,PCL}$). As expected, $T_{c,PCL}$ in the copolymer networks decreases progressively with decreasing PCL block molecular weight. In the subsequent heating scans (Fig. 1d), C_2, C_3 and C_4 samples display melting peaks between 45 °C and 55 °C, ascribed to the melting of the PCL crystal phase ($T_{m,PCL}$). Notably, a second, broader melting peak between 60 °C and 100 °C is observed, corresponding to the melting of the PBS crystalline phase ($T_{m,PBS}$).

Comparison of the $\chi_{c,PCL}$ and $\chi_{c,PBS}$ values between B and C samples reveals that both PCL and PBS phases exhibit marked reductions in crystallinity in the networks prepared from the triblock copolymers. In terms of overall crystalline content, the total PCL crystallinity in the C_series ranges from about 16% in C_1 to 33% in C_4, whereas the PBS crystalline fraction is significantly lower, decreasing from approximately 7.5% to 1.6% as the PCL block length increases (Table 2), which is consistent with a more integrated, PCL-dominated crystalline microstructure. Conversely, in B samples, the pronounced phase segregation conferred by the specific network architecture enhances crystallization. PBS crystallization is particularly suppressed in the copolymer networks (C samples), where PCL and PBS blocks are more intimately connected and evenly distributed, as reflected by the broad melting signals observed in this series of samples.

The thermal behavior of sample C_1 warrants separate consideration. This sample, characterized by comparatively short PCL blocks (2.7 kDa) and the highest PBS phase content (43 wt%), exhibits in the cooling scan a weak, broad exothermic signal composed of multiple peaks in the range −15 to 15 °C. Upon heating, a broad melting peak appears between 50 and 90 °C. In this sample, the crystallinity of the PCL segments is markedly reduced, due to both the limited block length and the chemical constraints imposed by the PBS blocks. Notably, the absence of exothermic crystallization signals above 30 °C in all C samples suggests that PBS crystallizes only at temperatures much lower than those of the neat PBS network, leading to overlap with the PCL crystallization region. Specifically, for samples with PCL block molecular weights greater than 2.7 kDa (C_2, C_3 and C_4), only a single crystallization peak is observed. As previously proposed for B_2 and B_3 specimens, PCL and PBS blocks in these copolymer networks may undergo coincident crystallization. A comparable behavior was reported by Safari et al.[25] for blends of PCL and poly(butylene succinate-*ran*-*ε*-caprolactone) random copolymers with different compositions. In their study, a melting peak associated with the copolymer BS units was detected regardless of blend composition, whereas no corresponding BS crystallization peak was observed. The authors attributed this behavior either to the coincident crystallization of BS and CL units or to cold crystallization of BS units during heating, whose signal might overlap with the melting of CL crystalline domains.

In the present work, the hypothesis of coincident crystallization of PCL and PBS in networks derived from PCL-PBS-PCL triblock copolymer is further supported by the close quantitative agreement between the crystallization enthalpies and the sum of the melting enthalpies measured in the subsequent heating scan (Table 2).

To further investigate the differences in thermal properties between the two series of networks, the crystallization behavior of representative samples B_2 and C_2 was examined using polarized optical microscopy (POM). Both samples possess similar PBS/PCL ratios, specifically 60/40 for B_2 and 66/34 for C_2, which enables a direct comparison of their crystallization behavior. Thin films were first heated to 130 °C to fully melt the crystalline domains and erase thermal history (Fig. 2a,d); subsequently, they were subjected to controlled cooling.

Remarkably, upon reaching temperatures near 80 °C, small spherulites became clearly observable in sample B_2. These structures are attributable to the formation of the PBS crystalline phase, as this temperature is well above the melting temperature of PCL. Maintaining the temperature constant, complete isothermal crystallization of PBS was observed, with the spherulites expanding omnidirectionally until the field of view was entirely occupied (Fig. 2b). Subsequently, upon reducing the temperature, a distinct morphological change was observed at approximately 35 °C, corresponding to the crystallization of PCL. Under isothermal conditions, PCL crystallization progressed over the previously formed PBS spherulites (Fig. 2c). This behavior is consistent with previous observations reported by Huang et al.[22] for PBS-*co*-PCL multiblock copolymers, in which the PBS component acts as a spherulitic superstructure, serving as a template that encapsulates and restricts the PCL phase. In contrast, during the cooling scan of the C_2 sample, no crystallization was detected above 35 °C (Fig. 2e). Only upon

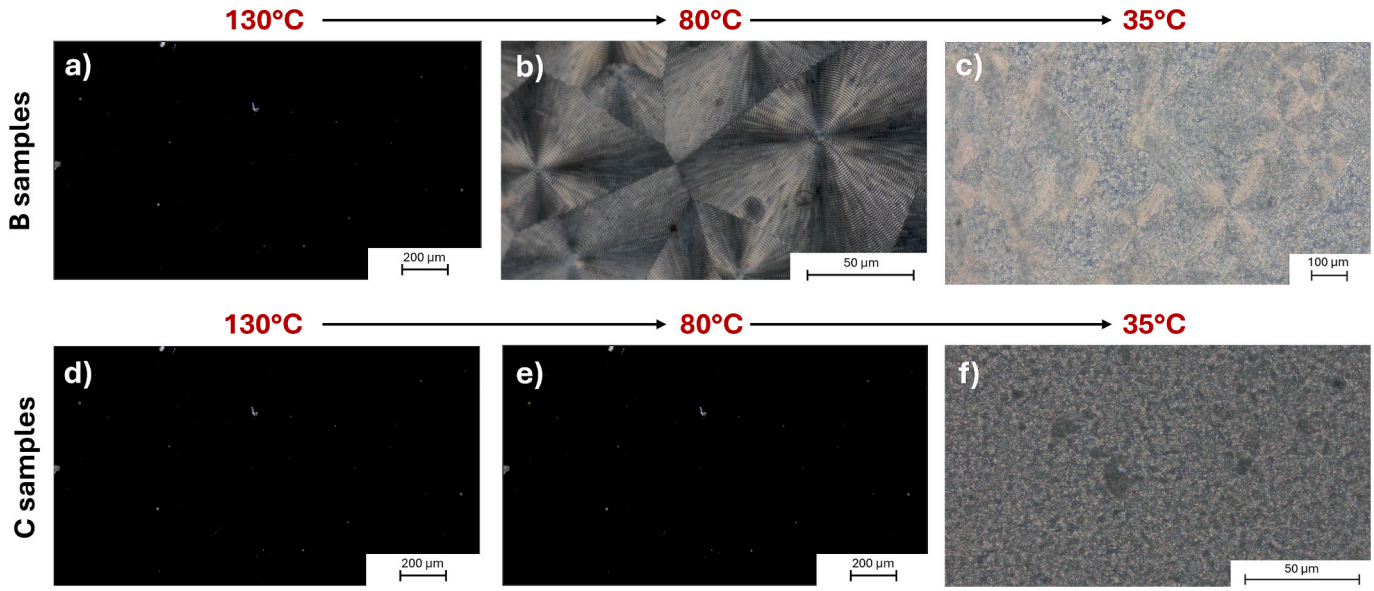

Fig. 2. POM images of B_2 sample (top row) and C_2 sample (bottom row). a, d) Melted state at 130 °C; b, e) isothermal crystallization at 80 °C; c, f) isothermal crystallization at 35 °C.

reaching this temperature, a birefringent crystalline phase appears (Fig. 2f). This outcome is consistent with differential scanning calorimetry (DSC) results and supports the hypothesis that, in sample C_2, during cooling, a coincident crystallization of the two components occurs.

DMTA analyses were performed to investigate the thermomechanical properties of the networks, with particular reference to the evolution of the storage modulus as a function of the temperature. To characterize both crystallization and melting phenomena, the tests were started from temperatures above the melting range, followed by controlled cooling below the crystallization temperature of both phases. A subsequent heating scan above the melting range was then performed. The results obtained for samples B_2, B_3, and B_4 of the B_series, and C_2, C_3, and C_4 of the C_series, are shown in Fig. 3a and 3b, respectively.

For the B_series, the cooling scans (dashed lines in Fig. 3a) show two distinct crystallization events, evidenced by increases in storage modulus at approximately 70 °C and 25 °C, which can be attributed to the crystallization of PBS and PCL blocks, respectively. Unlike DSC analysis, DMA measurements for samples B_3 and B_4 are sufficiently sensitive to resolve PBS crystallization separately from that of PCL, owing not only to the lower cooling rate adopted in DMA (3 °C min^{-1} vs. 20 °C min^{-1}), but also to the intrinsic sensitivity of mechanical measurements to small changes in crystalline fraction. During the heating ramps (solid lines), two distinct decreases in storage modulus are observed for all samples, centered at temperatures of approximately 65 °C and 125 °C, corresponding to the melting of PCL and PBS crystals, respectively. In all B samples, the melting transitions occur within the same temperature ranges regardless of sample composition, confirming the immiscibility of PBS and PCL phases, as already suggested by DSC analysis.

For the C_series, the cooling scans (dashed lines in Fig. 3b) indicate the crystallization at approximately 70 °C for C_4 and 40–50 °C for C_3 and C_2. In C_2, the increase in storage modulus is broad and continuous, whereas in C_3 and C_4 the modulus increases in a more discontinuous and broad fashion, characterized by two partially overlapping steps. This behavior is consistent with the hypothesis of nearly concurrent crystallization of PBS and PCL in the C samples. During the heating ramps (solid lines), the storage modulus decreases in two distinct steps, corresponding to the melting of PCL crystals followed by that of PBS crystals, although the two events are less clearly separated and extend over a broader temperature interval than in the B_series, in agreement with the DSC results.

In summary, the DMTA analysis highlights profound differences in the thermo-mechanical response of blend networks and triblock-based networks. In B samples, two well-separated drops of the storage modulus upon heating mirror the distinct melting of PCL and PBS crystals, respectively, leading to a pronounced intermediate plateau where only PBS crystals sustain the mechanical load. In contrast, C networks display a more gradual, monotonic decrease of the storage modulus over a broad temperature range, without a well-defined plateau, in line with the broadened and partially overlapping melting endotherms of PCL and PBS.

3.3. *One-way triple-shape-memory effect*

Polymeric networks containing multiple crystalline phases with distinct melting temperatures represent an advanced class of SMPs capable of exhibiting multiple, sequential shape-memory transitions. These systems can integrate several distinct switching phases, each with its own transition temperature, thus enabling programmable fixation and recovery of multiple temporary shapes within a single material.

The one-way triple-shape-memory effect of samples B and C was investigated using the thermo-mechanical cycle described in detail in the Experimental Section. Briefly, as illustrated schematically in Fig. 4a, the thermo-mechanical protocol enables the fixation of two temporary shapes (Shape I and Shape II) originating from the sample's original configuration (Shape O). Subsequently, two shape-memory transitions can be activated upon melting of the respective crystalline phases. The corresponding strain–temperature–stress evolution during the programming stage for representative B_4 and C_4 networks is provided in Fig. S8.

Fig. 4b and 4c present the recovery curves obtained by heating samples B and C, respectively, at a rate of 2 °C min^{-1} from −20 °C to T_{pr} (140 °C or 120 °C). The shape fixity parameter, R_{fix}, and the strain recoveries values, $R_{2\rightarrow1}$, $R_{1\rightarrow O}$ and R_{rec}, are summarized in Table 3.

All the samples exhibited very high strain fixity (R_{fix}) values around 99%. The B_series networks also displayed excellent overall strain recovery (R_{rec}) values, ranging between 97% and 99%, with recovery curves characterized by a distinct two-step profile (Fig. 4b). The first recovery step, $R_{II\rightarrow I}$, occurred between 50 °C and 65 °C as the PCL crystalline phase melted, whereas the second, $R_{I\rightarrow O}$, occurred in the

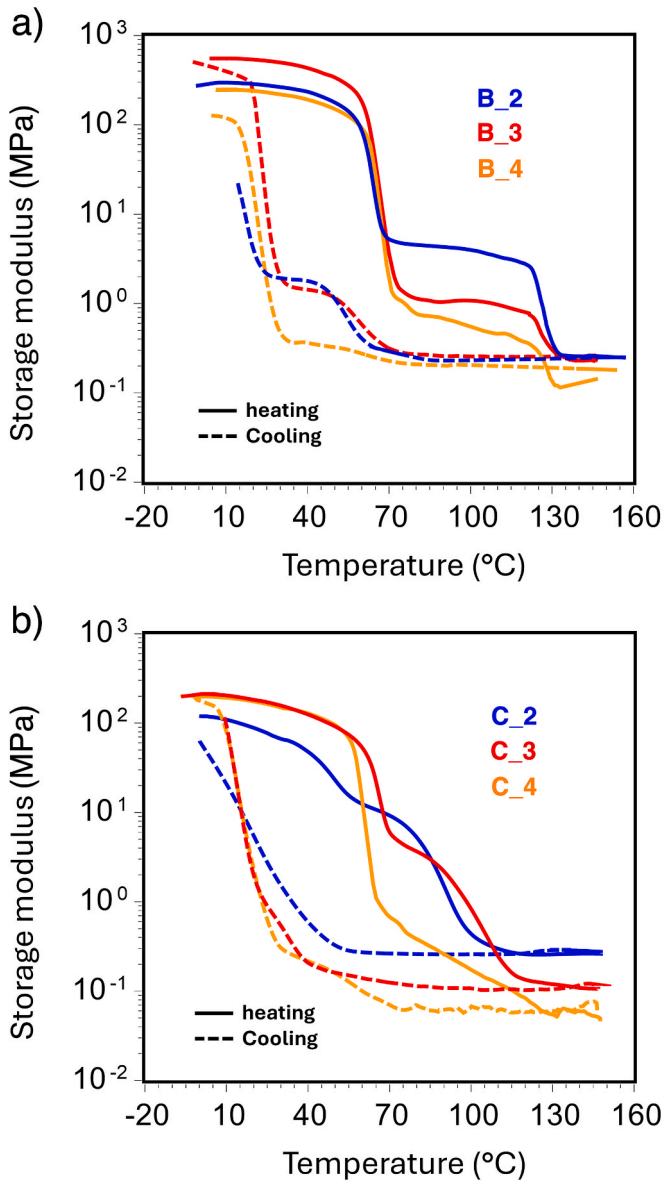

Fig. 3. DMTA analysis of B_samples (a) and C_samples (b). The dashed lines represent the cooling scans, whereas the solid lines represent the subsequent heating scans.

range of 110–130 °C, corresponding to the melting of the PBS crystalline domains.

During the programming cycle, the crystallization of the two phases is expected to fix the imposed deformation in each cooling step. Consequently, both the first and second strain recovery ratios were expected to reach approximately 50% of the imposed deformation, each corresponding to the 25% strain applied during the programming cycle (as visually suggested by the dashed line in Fig. 4b,c).

Notably, in B_series, all samples displayed a clear, well-defined double-step recovery (Fig. 4b), recovering between 36% and 61% of the applied deformation in the first recovery step (corresponding to a recovered strain between 18% and 30%, thus not far from what was expected). The two steps correspond to the melting of PCL and PBS, confirming that the two crystalline phases are segregated within the network. Notably, a larger PCL fraction within the network led to a more pronounced first-step recovery. Specifically, the measured values of $R_{II\rightarrow I}$ increased from 36% to 61%, and $R_{I\rightarrow O}$ decreased from 62% to 36% as the PCL content in the networks increased from 60 wt% (B_2) to 85 wt % (B_4). These outcomes suggest that the PBS phase has a detrimental effect during the first strain recovery. This effect may be attributed to the reduced chain mobility caused by the presence of the semi-crystalline and relatively rigid PBS phase within the amorphous PCL matrix. During the second recovery stage, once the PBS has melted, the chains being fully amorphous regain sufficient mobility.

Regarding the C samples, despite their high R_{fix} values, they exhibit lower R_{rec} compared to the B samples. Furthermore, the first and second recovery steps were not as distinctly separated as in the previous B samples (Fig. 4c). In the C_2 and C_3 networks, only a modest $R_{II\rightarrow I}$ (3% and 4%, respectively) was observed between 50 °C and 70 °C, followed by a broader recovery process extending from 70 °C to 120 °C, which ultimately leads to a residual deformation of about 4–5% of the applied strain (R_{rec} = 88 and 93%). The recovery curve of the C_4 network, by contrast, showed a first recovery step between 55 °C and 65 °C, accounting for 20% of the imposed strain (recovered strain about 10%). Subsequently, the remaining deformation ($R_{I\rightarrow O}$) was gradually recovered up to 120 °C, leading to a residual strain value close to that of the other C samples.

Overall, for the C samples, in which the PCL and PBS blocks crystallize in the same temperature range, only a limited recovery attributable to PCL melting was observed, even in the C_4 sample, which contains the highest PCL content. Evidently, in these specimens, the crystalline phase of PBS strongly restricts the chain mobility of PCL upon heating, even in networks with low PBS content, so that the restoration of the original shape occurs through a broad recovery process spanning a wide temperature range.

3.4. Two-way stress-free shape-memory

The two-way stress-free shape-memory effect was assessed by a thermo-mechanical testing protocol that enabled monitoring of the reversible strain evolution during cooling and heating cycles, following a programming procedure comprising the sequential steps shown in Fig. 5a. First, the sample was heated to the programming temperature T_{pr} (140 °C and 120 °C for the B and C series, respectively); second, it was elongated to 50% strain (A → B); third, under constant load, the sample was cooled to − 20 °C at a rate of 2 °C min^{-1} (B → C); finally, the load was removed (C → D). Subsequently, the two-way stress-free shape-memory effect was evaluated by heating the sample to the activation temperature T_{act} = 60–65 °C ($T_{m,PCL}$ + 15 °C) (D → E) and by performing thermal cycling between T_{act} and −20 °C at 2 °C min^{-1} under stress-free conditions (E ↔ F cycles). The reversible strain was evaluated in these latter cycles, consisting of a CIE upon cooling followed by a MIC upon heating.

Fig. 5a illustrates the programming step and the subsequent stress-free actuation cycle for samples B_4 and C_4, which have comparable PCL/PBS contents (85/15 for B_4 and 82/18 for C_4). The detailed strain–temperature–stress evolution during the entire programming sequence for these samples is reported in Fig. S9.

Table 4 summarizes the reversible elongations parameters (ε_{rev} and ε'_{rev}) obtained from cooling/heating cycles for both series B and C. As evident from Table 4 (and from Fig. 5a for B_4), the B samples exhibited negligible reversible shape changes in the two-way stress-free cycle; for instance, B_4 displayed ε_{rev} and ε'_{rev} values near 1%, which further declined in B_3 and became almost undetectable in B_2. In contrast, the networks prepared from triblock copolymers (C samples) displayed a marked reversible shape-memory response, with reversible elongation increasing with the PCL content. Specifically, ε_{rev} rose from approximately 2% for C_2 (66 wt% PCL) to 11% for C_4 (82 wt% PCL), while ε'_{rev} increased from 1% to 7%, indicating a clear positive correlation with the PCL content in the network. It should be noted that the two-way stress-free response was evaluated over a limited number of thermo-mechanical cycles (up to five cooling–heating cycles after programming), so that long-term cyclic durability and environmental ageing effects (e.g., humidity or chemical exposure) were not addressed in the present study.

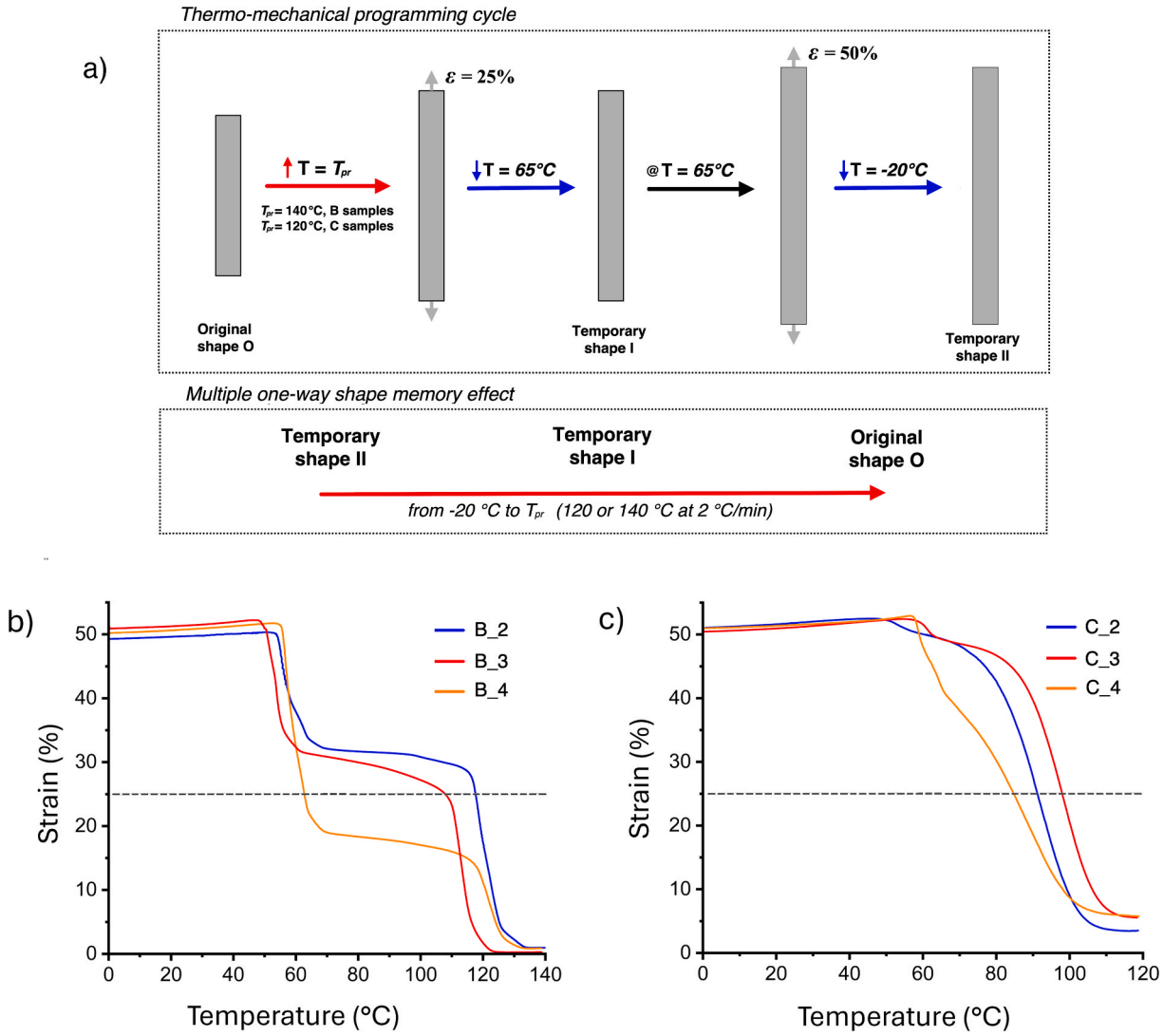

Fig. 4. a) Schematic representation of the thermo-mechanical programming cycle applied. recovery curves for samples B (b) and C (c), obtained by heating at 2 °C min^{-1} (dashed line represents the expected strain to be recovered in the first recovery process).

Table 3
Shape fixity R_{fix}, and the strain recovery parameters for samples B and C in one-way triple-shape-memory tests.

Sample code	R_{fix}[a] (%)	$R_{II\rightarrow I}$[b] (%)	$R_{I\rightarrow O}$[c] (%)	R_{rec}[d] (%)
B_2	99	36	62	98
B_3	98	39	60	99
B_4	99	61	36	97
C_2	99	3	90	93
C_3	99	4	84	88
C_4	99	20	68	88

[a] Determined using Equation 7;
[b] determined using Equation 8;
[c] determined using Equation 9;
[d] determined using Equation 10.

Based on these results, network C_4 (82/18 PCL/PBS wt ratio) was identified as the most promising material in terms of reversible shape-memory performance and was thus selected for subsequent characterization. The reversible elongations, ε_{rev} and ε'_{rev}, for this sample were quantitatively assessed as a function of the initial pre-stretch, which was systematically varied from 50% to 150%. The data are summarized in Table 5, and the corresponding strain vs time curves are shown in Fig. 5b.

The findings indicate that the reversible elongation, ε_{rev}, exhibits a moderate increase with increasing applied pre-stretch, ranging from approximately 11% to 16% for pre-stretch levels of 50 and 150%, respectively. In contrast, the reversible elongation, ε'_{rev}, remains essentially constant throughout the investigated pre-stretch interval, suggesting that, for all applied pre-stretch levels, the elongational strain occurring in the stress-free cycle is approximately a constant proportion (about 7%) of the strain the specimen experiences before the cycle.

The results highlight distinct differences in stress-free reversible behavior between the crosslinked B and C series. Networks synthesized from dimethacrylated triblock copolymers, particularly C_3 and C_4, exhibited a pronounced two-way shape-memory effect (2W-SME). In contrast, all networks based on dimethacrylated PCL/PBS macromonomers displayed negligible reversible actuation but excellent one-way triple-shape effect (1W-SME). To elucidate the origin of this different behavior, the material response during the cooling phase of the programming cycle, where crystallization proceeds under constant load, was examined.

Fig. 6 shows the strain evolution as a function of temperature during the programming step for the B (Fig. 6a) and C (Fig. 6b) samples, with specific reference to the early elongation as the initial strain is applied and the subsequent cooling induced elongation. In these experiments,

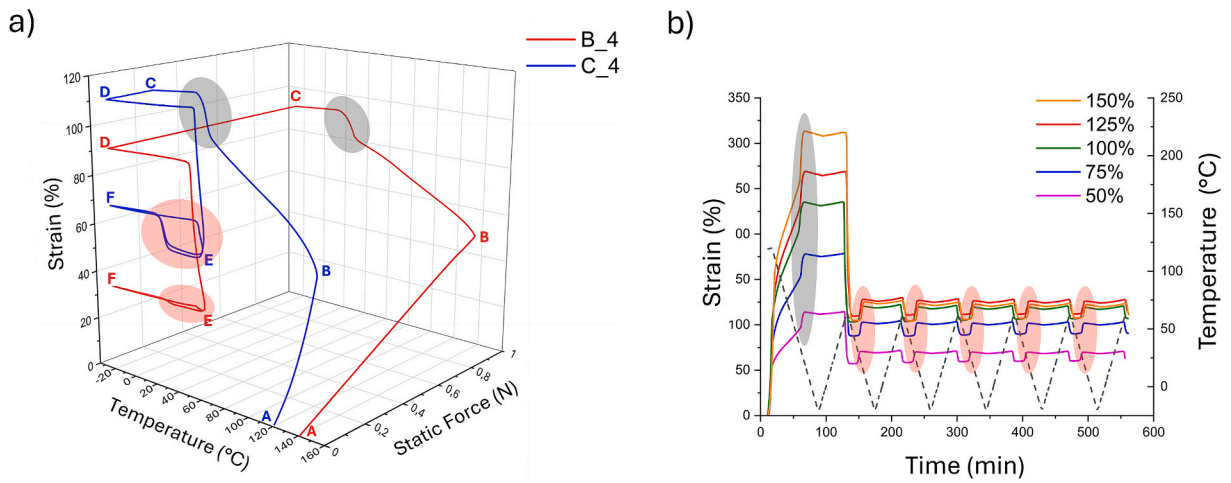

Fig. 5. a) Two-way stress-free shape memory cycles of B_4 (red) and C_4 (blue) programmed at the same pre-stretch of 50%; b) two-way stress-free shape memory response of C_4 over five cycles at different pre-stretch values. Shape changes associated with the stress-driven crystallization-induced elongation (CIE_{SD}) are highlighted in grey, whereas those related to the two-way stress-free effect are highlighted in red.

Table 4
Shape memory performance parameters in two-way stress-free shape memory tests for B and C samples.

Sample	ε_{rev} [a] (%)	ε'_{rev} [b] (%)	CIE_{SD} [b] (%)
B_2	0.2 ± 0.1	0.15 ± 0.1	1.5
B_3	0.9 ± 0.1	0.6 ± 0.1	4.0
B_4	1.0 ± 0.1	0.7 ± 0.1	8.5
C_2	1.8 ± 0.2	1.0 ± 0.1	2.5
C_3	6.2 ± 0.3	3.5 ± 0.2	7.0
C_4	10.9 ± 1.5	7.0 ± 0.9	17.0

[a] Elongation with respect to the initial sample length (Equation 11);
[b] elongation with respect to the sample length before the application of the stress-free cooling-heating cycle (Equation 12);
[c] stress-driven crystallization-induced elongation (Equation 13)

Table 5
Reversible elongations of sample C_4 obtained at different initial pre-stretch levels.

Pre-stretch	ε_{rev} [a](%)	ε'_{rev} [b](%)
50%	10.9 ± 1.5	7.0 ± 0.9
75%	12.3 ± 1.0	6.5 ± 0.6
100%	13.5 ± 1.5	6.5 ± 0.7
125%	14.7 ± 0.7	7.0 ± 0.4
150%	15.9 ± 1.1	7.6 ± 0.6

[a] Elongation with respect to the initial sample length (Equation 11);
[b] elongation with respect to the sample length before the application of the stress-free cooling-heating cycle (Equation 12).

the crosslinked specimens were first heated to the programming temperature T_{pr}, elongated to 50% of their initial length, and subsequently cooled under constant load to −20 °C at a rate of 2 °C min^{-1}. The resulting strain–temperature profiles reveal the occurrence of stress-driven crystallization-induced elongation, referred to as CIE_{SD} (Table 4), evidenced by discrete elongation steps within the cooling curves. When comparing these curves, it should be noted that imposing the same initial elongation required the application of different stress levels for the various samples (values reported in Fig. 6). Nevertheless, the applied load appears to play a minor role for both systems compared to their microstructural characteristics. This is particularly evident for the C_series samples, where markedly different elongational behaviors are observed among the networks under the same applied stress. By contrast, in the B_series samples, different loads are required to pre-stretch the material to the same initial strain; however, the resulting elongation is not strictly correlated with the applied stress. Thus, both the extent and the shape of the CIE-related portion of the curve provide insight into the different deformation and relaxation mechanisms activated during cooling, which are in turn, governed by the specific microstructural features of each network.

Remarkably, within the B_series, B_4 sample, containing the highest PCL fraction (85 wt%), exhibited the most pronounced CIE_{SD}, equal to 8.5%. In comparison, samples B_3 and B_2, with 75 wt% and 60% wt % PCL, displayed CIE_{SD} values of 4% and 1.5%, respectively. Furthermore, as shown in Fig. 6a, sample B_4 exhibited an almost linear increase in strain during cooling after being stretched to 50%, continuing until the onset of PCL crystallization-induced elongation. This behavior is consistent with rubber-like entropic elasticity, whereby the network becomes stiffer with increasing temperature, leading to gradual elongation upon cooling. Conversely, B_3 and B_2 exhibited entropy-driven elongation only up to approximately 80 °C, beyond which the strain plateaued. It is worth noting that PBS crystallization in the B_series typically occurs around 80 °C (Fig. 2b). In B_3 and B_2, containing 25 wt % and 40 wt% PBS, respectively, the extensive formation of PBS spherulites increases network stiffness, thereby restricting further elongation associated with subsequent PCL crystallization. Conversely, the lower PBS content in B_4 (15 wt%) allows the PCL chains to undergo more extensive elongation before and during crystallization.

The cooling curves corresponding to the C_series (Fig. 6b) revealed pronounced elongation during the cooling phase of thermo-mechanical programming, particularly for samples with higher PCL content. Specifically, sample C_4, containing 82 wt% PCL, exhibited a stress driven crystallization-induced elongation (CIE_{SD}) of 17% (Table 4). Similarly, sample C_3, with 77% wt % PCL, showed a CIE_{SD} of 7%, whereas C_2, with the lowest PCL amount (66 wt%) displayed only a modest elongation of 2.5%. It is important to note that both the C_4 and C_3 samples exhibited a significant entropic elongation (characterized by a linear increase of the strain) preceding the crystallization-induced elongation (CIE) of PCL. Conversely, in C_2, the linear entropic elongation persisted only up to approximately 35 °C, beyond which the strain remained nearly constant until reaching 10–15 °C, where a weak PCL-related CIE was observed. This behavior likely originates from partial PBS crystallization occurring in C_2 around 35 °C, a process that is not detectable by DSC analyses but facilitated here by the applied strain and reduced cooling rate.

In summary, samples B_4, C_3 and C_4 exhibited pronounced stress-driven CIE during the cooling stage of the programming cycle, whereas specimens B_3, B_2, and C_2 displayed suppressed CIE of PCL, primarily attributed to the earlier occurrence of PBS crystallization. Nevertheless,

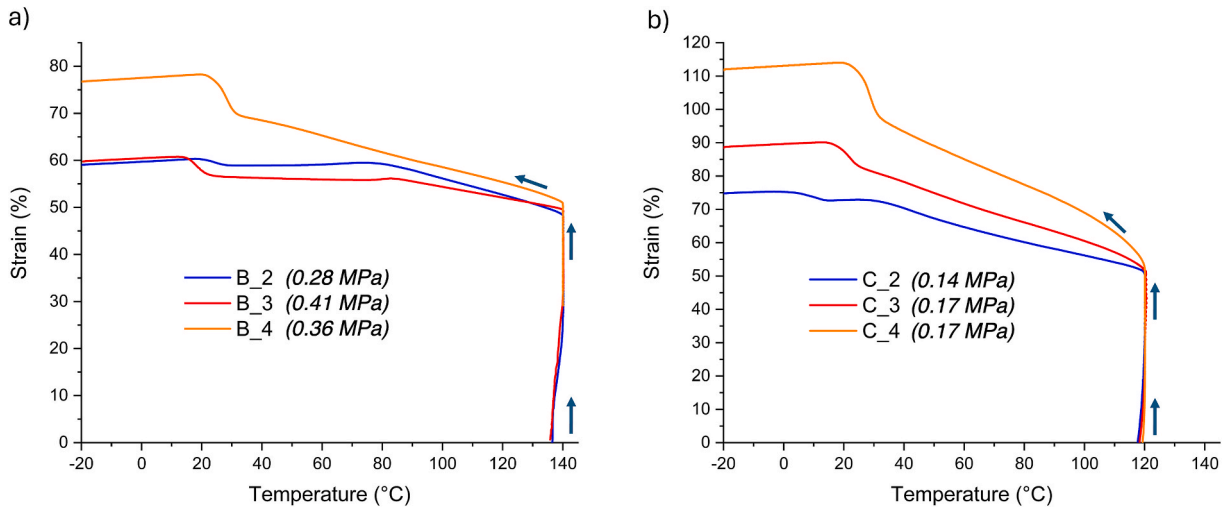

Fig. 6. Strain as a function of temperature during the cooling step of the programming cycle in two-way stress-free tests for a) B_series and b) C_series. The stress required to elongate the samples to 50% strain is reported in brackets.

only the C_series samples exhibited pronounced actuation, characterized by significant reversible elongations arising from CIE and MIC effects during thermo-mechanical cycles under stress-free conditions.

Recent findings by Liu et al.[26] demonstrated, by WAXD analysis of specifically prepared semicrystalline elastomers, that the key factor governing CIE in actuation domains is not merely the orientation of the crystalline phase, but rather the concomitant elongation and orientation of the amorphous phase during oriented crystallization. They quantified the amorphous orientation factor and showed that the orientation of the amorphous phase directly contributes to the macroscopic elongation jumps during crystallization–induced deformation. This literature evidence supports our interpretation that, in triblock–based networks (C_series), the covalent interphase connectivity and the resulting microstructure facilitate the transfer of crystallization–induced amorphous chain elongation into the pronounced stress–free actuation observed experimentally. In parallel, Wang and co-workers [27] reported that large crystallites within the skeleton domains induce pronounced stress relaxation in the surrounding matrix, causing those chains to realign into a compressed state. Conversely, smaller skeleton crystallites produce weaker stress relaxation, allowing amorphous chains in the actuation domains to remain oriented along the crystallization direction and thus to promote CIE upon cooling below T_c. Consequently, lower crystallinity and smaller crystallite size tend to enhance CIE, whereas higher crystallinity and larger crystallites inhibit it.

In this study, networks derived from photo-crosslinkable PCL and PBS macromonomers (B_series samples) permit independent crystallization of the immiscible and phase-segregated PCL and PBS domains. Consequently, during the programming stage of stress-free two-way shape-memory experiments (specifically, upon cooling from the melt), the molten PCL is confined within amorphous regions constrained by large PBS spherulites. This confinement restricts the elongation–contraction behavior of PCL, which serves as the actuation phase. Conversely, networks prepared from PCL–PBS–PCL triblock copolymer precursors (C_series samples) exhibit coincident crystallization of the two components, yielding smaller and less perfect crystallites. Upon shape-memory activation, these microstructural characteristics facilitate elongation of the molten PCL during cooling.

The overall crystalline fractions reported in Table 2 also support the different shape-memory responses of the two series. B networks retain substantial crystalline contents for both PCL and PBS, in line with their primary role as multi-step one-way (triple) SME systems. In contrast, C networks exhibit lower total crystallinity and a strongly reduced PBS crystalline fraction, indicative of a more integrated, PCL-dominated crystalline microstructure that is more conducive to internal-stress generation and thus correlates with the more efficient stress-free two-way actuation observed in this series.

In light of these results, the stress-free two-way response of the C_series networks can be rationalized in terms of an internal-stress mechanism governed by a skeleton/actuator morphology. In these triblock-based networks, PBS-rich domains form a comparatively stiff skeleton that remains at high modulus and partly crystalline within the temperature window where PCL melts and recrystallizes, while the covalent connectivity between PCL and PBS constrains the crystallization of the PCL blocks. During the programming step, cooling under load induces crystallization-induced elongation of the PCL phase in the presence of this PBS skeleton, so that a significant fraction of the imposed deformation cannot fully relax upon unloading and is stored as internal stress in the network. In the subsequent stress-free cooling/heating cycles, this stored internal stress biases PCL crystallization and melting along the pre-oriented direction, giving rise to reversible elongation on cooling and contraction on heating, whereas the PBS skeleton deforms only modestly and maintains the anisotropic internal stress field that sustains the two-way actuation over multiple cycles.

To further investigate the differences in elongation and orientation capability of the crystalline phases in the two sets of samples, the specimens' microstructures were examined by tapping-mode AFM on the free surface of the films, through the acquisition of both height and phase images (Fig. 7). In particular, the phase signal measures the phase shift between the cantilever driving stimulus and the response signal, where a phase lag arises from dissipative interactions between the oscillating tip and the sample surface. By this kind of analysis, the presence of materials or grains with different mechanical properties can be revealed.[28] Phase images were collected to track the evolution of the microstructure in B and C samples upon transition from an isotropic to an oriented state. B_2 and C_4 were selected as representative systems, corresponding to the less and the most effective two-way stress-free shape-memory networks, respectively. Specimens were prepared as follows: i) B_2 and C_4 samples were photo-crosslinked and subsequently analyzed without further treatments to preserve their isotropic state; ii) B_2_progr and C_4_progr samples were obtained starting from B_2 and C_4, respectively, heating them at T_{pr} (140 °C for B_2 and 120 °C for C_4), stretching to a 50% of strain before being cooled below $T_{c,PCL}$ under constant strain conditions to fix the programmed configuration.

As shown in Fig. 7, both B_2 (Fig. 7a) and C_4 (Fig. 7b) samples did not exhibit significant surface texturing and displayed nearly homogeneous mechanical properties. On the contrary, B_2_progr (Fig. 7c) and C_4_progr (Fig. 7d) showed barely noticeable and well-defined

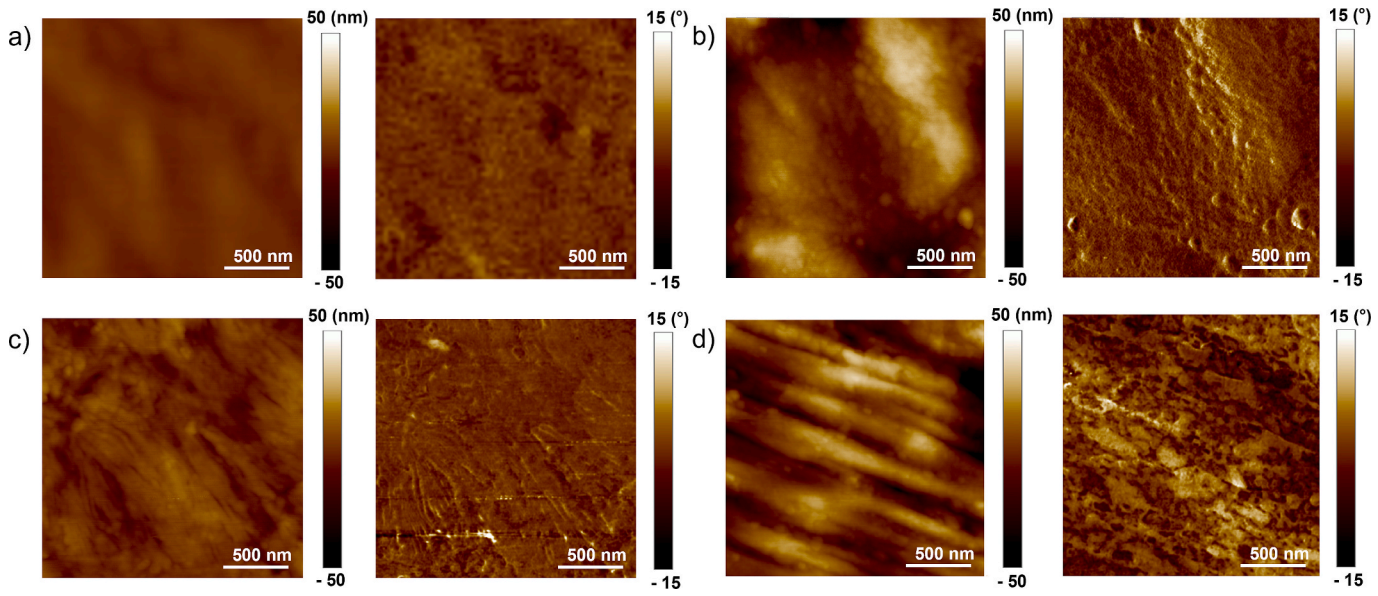

Fig. 7. Results of AFM analysis. Each couple of images represent height (left) and phase (right) signals for a) B_2, b) C_4, c) B_2_progr and d) C_4_progr.

anisotropic topographical features, respectively. The latter can be ascribed to the onset of micro sized crystalline domains, especially evident in the C_4_progr sample. Notably, the phase signal of C_4_progr clearly shows the presence of elongated grains exhibiting distinct mechanical properties. The absence of correlation between the phase and height signals strongly suggests the presence of areas with distinct viscoelastic properties in the C_4_progr sample compared to the other investigated samples.

Based on these findings, microstructural analyses of B_2_progr and C_4_progr revealed that sample C_4 exhibited a more pronounced and well-defined orientation of the semicrystalline domains than sample B_2 after programming. This result further substantiates the hypothesis that, in networks derived from the photo-crosslinking of PCL and PBS macromonomer blends, the crystallization of PBS restricts the orientation of the PCL crystalline phase.

It is widely recognized that the stress-free reversible SME relies on efficient stress transfer from the oriented crystallites in the skeleton phase to the molten chains in the actuation phase. If these two phases remain largely independent and interfacial interactions are minimal, the oriented skeleton phase cannot induce elongation of the actuation phase upon cooling. In B_series samples, the segregation of the crystalline PCL and PBS phases prevents the establishment of strong interfacial interactions. By contrast, in C_series samples, in which covalent bonds link the PCL and PBS blocks, exhibit strong interphase coupling that markedly enhances stress transfer from the oriented skeleton phase to the PCL actuation phase within the network.

This hypothesis is corroborated by the findings of Gao et al.[29,30] on polyolefin blends, which demonstrated that a two-way stress-free shape memory effect is promoted in blends that exhibit shifts in the melting peaks of the constituent polymers compared to their pure homopolymer forms. These shifts were attributed to inter-chain mixing and the formation of interfacial crystalline domains between the different components. Interestingly, the authors also noted that crystallites of the actuation and skeleton phases with markedly different sizes may hinder stress transfer between the phases, thereby limiting the reversible shape-memory effect under both in stress-free and under load conditions.

4. Conclusions

In this work, chemically crosslinked polymer networks containing multiple semicrystalline phases were successfully prepared through two complementary strategies: (i) blending photo-crosslinkable PCL and PBS macromonomers (B_series), and (ii) photo-crosslinking dimethacrylated PCL–PBS–PCL triblock copolymers (C_series) with tailored block lengths and compositions. Although both systems share a similar chemical composition, they exhibit distinctly different thermal, morphological, and shape-memory behaviors.

DSC, DMTA and polarized optical microscopy revealed that the B_series networks possess well-separated PCL and PBS crystalline domains with independent crystallization and modulus, which is key to enabling a robust multi-step shape-memory response. In comparison, the C_series networks exhibit a more gradual, monotonic decrease of the storage modulus over a broad temperature range, without a well-defined plateau, which is consistent with the broadened and partially overlapping melting endotherms of PCL and PBS arising from coincident crystallization and the formation of mixed, partially co-crystalline regions that yield a more integrated phase behavior.

As a result, the B_series samples displayed a clear two-step melting and crystallization process, enabling a well-defined one-way triple-shape-memory effect characterized by excellent strain fixity and nearly complete recovery, yet negligible reversible actuation. Conversely, the C_series networks demonstrated significantly enhanced two-way stress-free shape-memory performance, stemming from their more homogeneous morphology and stronger interphase coupling. These materials exhibited reversible elongations up to 16% under thermal cycling, with actuation amplitude tunable through the initial programming strain. AFM analysis confirmed that, upon programming, C samples developed more oriented semicrystalline domains that facilitate efficient stress transfer between the skeleton and actuation phases. The covalent linkage between PCL and PBS blocks promoted strong interfacial interactions, thereby enhancing stress-induced crystallization and melting-induced contraction.

Overall, this study highlights the crucial role of interphase coupling and crystallization dynamics in governing the actuation behavior of semicrystalline shape-memory polymer networks. Networks with covalently connected and partially miscible crystalline phases, such as those in the C_series, enable efficient stress transfer and pronounced reversible actuation, whereas highly phase-segregated networks, such as the B_series, are more suitable for achieving multi-step one-way (triple) shape-memory effects. These findings provide valuable design guidelines for next-generation semicrystalline SMPs capable of tunable and reversible actuation under stress-free conditions. At the same time, a systematic assessment of long-term cycling stability and performance

under relevant environmental conditions will be required in future work to support their implementation in real applications such as soft robotics or smart textiles.

CRediT authorship contribution statement

Daniele Natali: Writing – review & editing, Writing – original draft, Visualization, Validation, Methodology, Investigation, Formal analysis, Data curation, Conceptualization. **Chiara Gualandi:** Writing – review & editing, Writing – original draft, Visualization, Supervision, Resources, Project administration, Methodology, Investigation, Formal analysis, Conceptualization. **Michele Bianchi:** Writing – review & editing, Validation, Methodology, Investigation, Formal analysis, Conceptualization. **Andrea Alessandrini:** Writing – review & editing, Validation, Methodology, Investigation, Formal analysis, Conceptualization. **Stefano Pandini:** Writing – review & editing, Methodology, Investigation, Formal analysis, Conceptualization. **Michele Zanoni:** Writing – review & editing, Methodology, Investigation, Formal analysis, Conceptualization. **Maria Letizia Focarete:** Writing – review & editing, Methodology, Formal analysis, Conceptualization. **Maurizio Toselli:** Writing – review & editing, Writing – original draft, Visualization, Supervision, Resources, Project administration, Methodology, Investigation, Funding acquisition, Formal analysis, Conceptualization.

Declaration of competing interest

The authors declare that they have no known competing financial interests or personal relationships that could have appeared to influence the work reported in this paper.

Acknowledgements

The authors gratefully acknowledge the European Laboratory for Non-Linear Spectroscopy (LENS), University of Florence, for performing the polarized optical microscopy (POM) measurements used to characterize the sample morphology. The authors also thank Dr Daniele Martella and Dr Marco Turriani for their technical assistance and insightful discussions.

This work was supported by the National Recovery and Resilience Plan (PNRR), Italy, through the National Center for Sustainable Made in Italy (Project PE11 “MICS”, Spoke 4.07 “ROOTS: gReen sOft rOboTicS”). This project is funded by the European Union – NextGenerationEU.

Appendix A. Supplementary data

Supplementary data to this article can be found online at https://doi.org/10.1016/j.eurpolymj.2026.114688.

Data availability

Data will be made available on request.

References

[1] L. Sun, W.M. Huang, Z. Ding, Y. Zhao, C.C. Wang, H. Purnawali, C. Tang, Stimulus-responsive shape memory materials: a review, Mater. Des. 33 (2012) 577–640, https://doi.org/10.1016/j.matdes.2011.04.065.

[2] L. Yang, J. Lou, J. Yuan, J. Deng, A review of shape memory polymers based on the intrinsic structures of their responsive switches, RSC Adv. 11 (2021) 28838–28850, https://doi.org/10.1039/D1RA04434F.

[3] L. Luo, F. Zhang, L. Wang, Y. Liu, J. Leng, Recent advances in shape memory polymers: multifunctional materials, multiscale structures, and applications, Adv. Funct. Mater. 34 (2024), https://doi.org/10.1002/adfm.202312036.

[4] M. Herath, J. Epaarachchi, M. Islam, L. Fang, J. Leng, Light activated shape memory polymers and composites: a review, Eur. Polym. J. 136 (2020) 109912, https://doi.org/10.1016/j.eurpolymj.2020.109912.

[5] X. Zhang, W. Tang, D. Yang, J. Ma, X. Li, G. Tian, The latest advances in two-way shape memory polymers: fabrication strategies, programming mechanisms, and emerging applications, Chem. Eng. J. 521 (2025), https://doi.org/10.1016/j.cej.2025.166372.

[6] Y.Y. Yu, H.P. Xiang, L.F. Fan, M.Q. Zhang, Shape memory elastomers: a review of molecular structures, stimulus mechanisms, and emerging applications, Poly. Sci. Technol. 1 (2025) 271–298, https://doi.org/10.1021/polymscitech.4c00035.

[7] K. Wang, Y.G. Jia, C. Zhao, X.X. Zhu, Multiple and two-way reversible shape memory polymers: design strategies and applications, Prog. Mater Sci. 105 (2019), https://doi.org/10.1016/j.pmatsci.2019.100572.

[8] M. Behl, K. Kratz, J. Zotzmann, U. Nöchel, A. Lendlein, Reversible bidirectional shape-memory polymers, Adv. Mater. 25 (2013) 4466–4469, https://doi.org/10.1002/adma.201300880.

[9] K. Wang, Y.G. Jia, X.X. Zhu, Two-way reversible shape memory polymers made of cross-linked cocrystallizable random copolymers with tunable actuation temperatures, Macromolecules 50 (2017) 8570–8579, https://doi.org/10.1021/acs.macromol.7b01815.

[10] S.M. Lai, S.Y. Fan Jiang, H.C. Chou, T.Y. Lin, Y.E. Wei, B.Y. Yu, Novel two-way multiple shape memory effects of olefin block copolymer (OBC)/polycaprolactone (PCL) blends, Polym Test 102 (2021), https://doi.org/10.1016/j.polymertesting.2021.107333.

[11] S.M. Lai, T.Y. Lin, G.L. Huang, A novel multi-triggered reversible shape memory thermoplastic polyurethane (TPU)/polycaprolactone (PCL) blend, J. Polym. Res. 30 (2023), https://doi.org/10.1007/s10965-022-03420-9.

[12] N. Inverardi, M. Toselli, G. Scalet, M. Messori, F. Auricchio, S. Pandini, Stress-free two-way shape memory effect of poly(ethylene glycol)/poly(ε-caprolactone) semicrystalline networks, Macromolecules 55 (2022) 8533–8547, https://doi.org/10.1021/acs.macromol.2c01064.

[13] Q. Guo, Y. Zhang, H. Ruan, H. Sun, T. Wang, Q. Wang, C. Wang, Solvent content controlling strategy for cocrystallizable polyesters enables a stress-free two-way shape memory effect with wider service temperatures, Macromol. Rapid Commun. 45 (2024), https://doi.org/10.1002/marc.202300534.

[14] J.M. Cuevas, R. Rubio, L. Germán, J.M. Laza, J.L. Vilas, M. Rodriguez, L.M. León, Triple-shape memory effect of covalently crosslinked polyalkenamer based semicrystalline polymer blends, Soft Matter 8 (2012) 4928–4935, https://doi.org/10.1039/c2sm07481h.

[15] F.K. Molavi, I. Ghasemi, M. Messori, M. Esfandeh, Design and characterization of novel potentially biodegradable triple-shape memory polymers based on immiscible Poly(l-lactide)/Poly(ε-caprolactone) blends, J. Polym. Environ. 27 (2019) 632–642, https://doi.org/10.1007/s10924-019-01366-6.

[16] Y. Wang, L. Huang, X. Wang, X. Lu, B. Wang, Y. Qin, C. Huang, Photoresponsive triple shape memory polymers with a self-healing function based on poly (lactic acid)/polycaprolactone blends, Polym. Test. 120 (2023), https://doi.org/10.1016/j.polymertesting.2023.107966.

[17] A. Fernández-Tena, R.A. Pérez-Camargo, O. Coulembier, L. Sangroniz, N. Aranburu, G. Guerrica-Echevarria, G. Liu, D. Wang, D. Cavallo, A.J. Müller, Effect of molecular weight on the crystallization and melt memory of Poly (ϵ-caprolactone) (PCL), Macromolecules 56 (2023) 4602–4620, https://doi.org/10.1021/acs.macromol.3c00234.

[18] Y. Zhang, T. Li, Z. Xie, J. Han, J. Xu, B. Guo, Synthesis and properties of biobased multiblock polyesters containing Poly(2,5-furandimethylene succinate) and Poly (butylene succinate) blocks, Ind. Eng. Chem. Res. 56 (2017) 3937–3946, https://doi.org/10.1021/acs.iecr.7b00516.

[19] M. Messori, M. Degli Esposti, K. Paderni, S. Pandini, S. Passera, T. Riccò, M. Toselli, Chemical and thermomechanical tailoring of the shape memory effect in poly (ε-caprolactone)-based systems, J. Mater. Sci. 48 (2013) 424–440, https://doi.org/10.1007/s10853-012-6757-8.

[20] T. Miyata, T. Masuko, Crystallization behaviour of poly(tetramethylene succinate), Polymer (guildf) 39 (1998) 1399–1404, https://doi.org/10.1016/S0032-3861(97)00418-7.

[21] V. Crescenzi, G. Manzini, G. Calzolari, C. Borri, Thermodynamics of fusion of poly-β-propiolactone and poly-ϵ-caprolactone. comparative analysis of the melting of aliphatic polylactone and polyester chains, Eur. Polym. J. 8 (1972) 449–463, https://doi.org/10.1016/0014-3057(72)90109-7.

[22] M. Huang, X. Dong, L. Wang, L. Zheng, G. Liu, X. Gao, C. Li, A.J. Müller, D. Wang, Reversible lamellar periodic structures induced by sequential crystallization/melting in PBS-co-PCL multiblock copolymer, Macromolecules 51 (2018) 1100–1109, https://doi.org/10.1021/acs.macromol.7b01779.

[23] Z. Qiu, M. Komura, T. Ikehara, T. Nishi, Miscibility and crystallization behavior of biodegradable blends of two aliphatic polyesters. Poly(butylene succinate) and Poly(ε-caprolactone), Polymer (guildf) 44 (2003) 7749–7756, https://doi.org/10.1016/j.polymer.2003.10.013.

[24] S.E. Fenni, J. Wang, N. Haddaoui, B.D. Favis, A.J. Müller, D. Cavallo, Crystallization and self-nucleation of PLA, PBS and PCL in their immiscible binary and ternary blends, Thermochim Acta 677 (2019) 117–130, https://doi.org/10.1016/j.tca.2019.03.015.

[25] M. Safari, R.A. Pérez-Camargo, L. Ballester-Bayarri, G. Liu, A. Mugica, M. Zubitur, D. Wang, A.J. Müller, Biodegradable binary blends of poly (butylene succinate) or poly (ε-caprolactone) with poly (butylene succinate-ran-ε-caprolactone) copolymers: crystallization behavior, Polymer (guildf) 256 (2022), https://doi.org/10.1016/j.polymer.2022.125206.

[26] W. Liu, J.P. Qu, J. Wang, Z. Tu, H. Zhang, M.M. Wang, Actuation mechanisms of a semicrystalline elastomer-based polymer artificial muscle with high actuation strain, Macromolecules 55 (2022) 3986–3999, https://doi.org/10.1021/acs.macromol.2c00549.

[27] J. Wang, H. Zhang, J. Lei, M. Wu, W. Liu, J.P. Qu, Stress-free two-way shape-memory mechanism of a semicrystalline network with a broad melting transition,

Macromolecules 55 (2022) 10113–10123, https://doi.org/10.1021/acs.macromol.2c01971.
[28] J. Tamayo, R. García, Deformation, contact time, and phase contrast in tapping mode scanning force, Langmuir 12 (1996) 4430–4435, https://doi.org/10.1021/la960189l.
[29] Y. Gao, W. Liu, S. Zhu, Thermoplastic polyolefin elastomer blends for multiple and reversible shape memory polymers, Ind. Eng. Chem. Res. 58 (2019) 19495–19502, https://doi.org/10.1021/acs.iecr.9b03979.
[30] Y. Gao, W. Liu, S. Zhu, Polyolefin thermoplastics for multiple shape and reversible shape memory, ACS Appl. Mater. Interf. 9 (2017) 4882–4889, https://doi.org/10.1021/acsami.6b14728.